

Critical dynamics of the nonconserved strongly anisotropic permutation symmetric three-vector model

Rajiv G. Pereira

School of Physics, IISER Thiruvananthapuram, Vithura, Kerala 695551, India



(Received 11 September 2020; accepted 20 November 2020; published 29 December 2020)

We explore, employing the renormalization-group theory, the critical scaling behavior of the permutation symmetric three-vector model that obeys *nonconserving* dynamics and has a relevant anisotropic perturbation which drives the system into a nonequilibrium steady state. We explicitly find the independent critical exponents with corrections up to two loops. They include the static exponents ν and η , the off equilibrium exponent $\tilde{\eta}$, the dynamic exponent z , and the strong anisotropy exponent Δ . We also express the other anisotropy exponents in terms of these.

DOI: [10.1103/PhysRevE.102.062150](https://doi.org/10.1103/PhysRevE.102.062150)

I. INTRODUCTION

Universality exhibited by systems out of equilibrium has been a prominent object of study in statistical physics, especially since the formulation of the renormalization-group (RG) theory [1–4]. A variety of genuine nonequilibrium (NE) universality classes have been identified and well studied in the past few decades. The driven diffusive systems [2,5,6] and the percolation models [7,8] are a few examples. However, in comparison to equilibrium and near-equilibrium classes [9,10], genuine nonequilibrium ones remain far less explored.

Driven-diffusive models constitute an important category that violates the detailed-balance condition. They have been widely used to describe physical systems, such as fast ionic conductors [11,12] and traffic jams [13,14], in order to investigate physics far from equilibrium. A variety of such models have been explored in the past [5], and they continue to appear in recent studies, for instance, Bose condensation transition [15,16] and systems coupled to mutually interacting Langmuir kinetics [17]. These are essentially Ising-like models with anisotropic forces, and many of them exhibit universality distinct from that of any equilibrium class [18–20]. However, those models with spatially biased forces that violate detailed balance even at the long-distance and large-time limit are mostly the ones that follow conserving dynamics.

Nonconserved Ising-like systems with relevant anisotropic perturbations are rare, and their critical properties are far less explored. One such exception can be found in Ref. [21], wherein a cyclic permutation symmetric three-vector model with nonconserving dynamics and anisotropic perturbations was introduced. It was shown that for this model, below the critical dimension $d_c = 4$, there exists an infrared stable fixed point at which one of the anisotropic perturbations is relevant, thus identifying a genuine nonequilibrium universality class.

Though the anisotropic NE fixed point was identified, the critical behavior of this class has not been investigated. Secondly, the relevance of the anisotropic term should reflect as difference in the longitudinal and the transverse power-law behavior of the correlation functions. Further, unlike other commonly found Ising-like systems with relevant spatial bias

[18–20,22,23], this model follows nonconserving dynamics. These factors raise several interesting questions. What are the similarities and the differences in the critical behavior of the model from that of the conserved ones? Does the model exhibit common critical features such as faster decay of longitudinal fluctuations [5]? Is the critical power-law decay of the response and the correlation functions spatially biased?

Motivated by these questions, we explore the critical scaling behavior of this class. For this, we look at a simpler model obtained by replacing the cyclic permutation symmetry in the model introduced in Ref. [21] by permutation symmetry. In other words, we consider the nonconserved strongly anisotropic permutation symmetric (NSAPS) three-vector model. It is sufficient to study this model and determine the critical exponents as it has the same NE fixed point. To this end, we perform a two-loop RG analysis on this model.

We organize this paper as follows. In Sec. II, we introduce the NSAPS three-vector model. In Sec. III, we first discuss the renormalization of the theory and then briefly describe the computational methods employed in the two-loop calculation. In Sec. IV, we obtain the critical exponents to two-loop order in an expansion around the upper critical dimension $d_c = 4$ and then discuss the various critical features of the model. In Appendix A, the computational methods used in obtaining and evaluating the Feynman diagrams are detailed, and in Appendices B to I the relevant one particle irreducible (1PI) diagrams and their divergences are listed.

II. THE MODEL

The most general field theory for nonconserved N -vector models subject to anisotropic forces with all the marginal perturbations in $4 + 1$ dimensions was constructed in Ref. [21]. The theory is written in Martin-Siggia-Rose (MSR) formalism [24] as

$$\mathcal{S}(\phi, \tilde{\phi}) = \int_x [\tilde{\phi}_a(\partial_t - \nabla^2 + r)\phi_a - \frac{1}{2}\mathcal{E}_{abc}\tilde{\phi}_a\phi_b\partial_{||}\phi_c + \frac{1}{3!}G_{abcd}\tilde{\phi}_a\phi_b\phi_c\phi_d - T\tilde{\phi}_a\tilde{\phi}_a], \quad (1)$$

where x denotes the time and the space coordinates $\{t, \mathbf{x}\}$, $\int_x \equiv \int dt d^d \mathbf{x}$, $\tilde{\phi}$ is the auxiliary field, and T is the noise strength. The fields ϕ and $\tilde{\phi}$ are functions of x and the repeated indices are summed over. The G terms are straightforward generalizations of the ϕ^4 term in the familiar $O(n)$ symmetric relaxational models [2,25]. The \mathcal{E} terms are genuine nonequilibrium anisotropic perturbations which violate detailed balance. Such perturbations do not allow the system to equilibrate at large time, leading to nonequilibrium states which exhibit several interesting properties [26,27].

It was shown in Ref. [21] that only when the number of components $N = 3$ there can be anisotropic perturbations consistent with a single length scale. In the case of cyclic permutation symmetry, there are five allowed independent couplings, namely, G_{1111} , G_{1122} , G_{1133} , \mathcal{E}_{123} , and \mathcal{E}_{132} . Below the upper critical dimension $d_c = 4$ this model has an infrared stable NE fixed point at which the anisotropic coupling \mathcal{E}_{123} and the couplings G_{1111} and G_{1122} are relevant, while the couplings G_{1133} and \mathcal{E}_{132} are irrelevant [21]. Thus, a nonconserved Ising-like model with a relevant anisotropic perturbation was constructed, identifying a genuine nonequilibrium universality class.

If we now restrict to full permutation symmetry, the NSAPS three-vector model is obtained, where the number of allowed independent couplings reduces to three, namely, G_{1111} , G_{1122} , and \mathcal{E}_{123} . Note that permutation symmetry does not distinguish G_{1133} and \mathcal{E}_{132} from G_{1122} and \mathcal{E}_{123} , respectively. The NSAPS three-vector model has the same infrared stable fixed point as the cyclic permutation symmetric one [21]. Therefore, it is sufficient to study the critical scaling behavior of this model. The MSR action for this simpler case can be written as

$$S = \sum_{a=1}^3 \int_x \left\{ \tilde{\phi}_a [\partial_t - D(\nabla_{\perp}^2 + \rho \partial_{\parallel}^2 - r)] \phi_a - T \tilde{\phi}_a^2 + \frac{u_0}{3!} \tilde{\phi}_a \phi_a^3 + \frac{u_1}{2!} \tilde{\phi}_a \phi_a (\phi_{a+1}^2 + \phi_{a+2}^2) + e_p \phi_{a+1} \phi_{a+2} \partial_{\parallel} \tilde{\phi}_a \right\}, \quad (2)$$

where $u_0 \equiv G_{1111}$, $u_1 \equiv G_{1122}$, $e_p \equiv \mathcal{E}_{123}$, $\phi_{i+3} \equiv \phi_i$, and $\tilde{\phi}_{i+3} \equiv \tilde{\phi}_i$. We split the ∇^2 term into the longitudinal and the transverse components by introducing the coefficient ρ as the theory is spatially anisotropic.

By setting $\phi_i = \phi$, for $i = 1, 2$, and 3 , and $u_1 = u_0/(3!)$ in Eq. (2), we obtain the one-component model which was studied by Bassler and Schmittmann [28]. This special case can be thought of as a coarse-grained model describing particles hopping on an Ising lattice subject to an anisotropic force, $e_p \partial_{\parallel} \phi^2$, where the number of particles is not conserved.

We proceed to perform a two-loop RG analysis on the NSAPS three-vector model and extract the critical exponents associated to the response and the correlation functions.

III. RG ANALYSIS

In this section, we first discuss the standard renormalization procedure (see, for example, the excellent textbook by Täuber [2]), and apply it to the NSAPS three-vector model, where we define the renormalization constants and state the

renormalization conditions. Then we briefly describe the computational techniques employed in the calculation, which are suitable when the diagrams are numerous. The computational packages FEYNARTS [29] and FEYNALCALC [30,31] are used with MATHEMATICA [32] to obtain the Feynman diagrams and the package SECDEC [33] is used for numerical dimensional regularization.

A. Definitions and notations

The effective action is written as

$$\Gamma[\psi, \tilde{\psi}] = -\ln \mathcal{Z}[J, \tilde{J}] + \sum_a \int_x J_a(x) \psi_a(x) + \tilde{J}_a(x) \tilde{\psi}_a(x), \quad (3)$$

where $\psi(x) = \frac{\delta \ln \mathcal{Z}}{\delta J(x)}$, $\tilde{\psi}(x) = \frac{\delta \ln \mathcal{Z}}{\delta \tilde{J}(x)}$, and the generating functional for correlation functions $\mathcal{Z}[J, \tilde{J}] = \langle \exp \sum_a \int_x \phi_a(x) J_a(x) + \tilde{\phi}_a(x) \tilde{J}_a(x) \rangle$. The 1PI diagrams are obtained by taking the functional derivatives of Γ :

$$\Gamma_{\tilde{n}, n}^{\tilde{a}_1 \dots \tilde{a}_n a_1 \dots a_n}(\tilde{x}_1, \dots, \tilde{x}_n; x_1, \dots, x_n) = \prod_{i=1}^{\tilde{n}} \frac{\delta}{\delta \tilde{\psi}_{\tilde{a}_i}(\tilde{x}_i)} \prod_{j=1}^n \frac{\delta}{\delta \psi_{a_j}(x_j)} \Gamma[\tilde{\psi}, \psi] \Big|_{\tilde{\psi}=\psi=0}. \quad (4)$$

The ultraviolet divergences are absorbed into the renormalization constants Z_{ϕ} , $Z_{\tilde{\phi}}$, Z_D , Z_{ρ} , Z_T , Z_0 , Z_1 , and Z_p , and the bare fields and the bare parameters are written in terms of their renormalized counterparts as

$$\begin{aligned} \phi_a &= Z_{\phi}^{1/2} \phi_{aR}, \quad \tilde{\phi}_a = Z_{\tilde{\phi}}^{-1/2} \tilde{\phi}_{aR}, \quad D = \frac{Z_D}{Z} D_R, \\ \rho &= \frac{Z_{\rho}}{Z_D} \rho_R, \quad T = \frac{Z_T}{Z_{\tilde{\phi}}} T_R, \quad r = \frac{Z_r}{Z_D} \mu^2 r_R, \\ u_0 &= \frac{Z_0}{ZZ_{\phi}} u_{0R}, \quad u_1 = \frac{Z_1}{ZZ_{\phi}} u_{1R}, \quad e_p = \frac{Z_p}{ZZ_{\phi}^{1/2}} e_{pR}, \end{aligned} \quad (5)$$

where $Z = \sqrt{Z_{\phi} Z_{\tilde{\phi}}}$, the subscript R denotes the renormalized quantities, and the factor μ is introduced to make r_R dimensionless. The renormalization constants are fixed by the following renormalization conditions with the minimal subtraction scheme:

$$\Gamma_{R, 1, 1}^{11}(q_i = 0) = D_R r_R \mu^2, \quad (6)$$

$$\left. \frac{\partial}{\partial q_{\parallel}^2} \Gamma_{R, 1, 1}^{11}(q; q) \right|_{q=0} = D_R \rho_R, \quad (7)$$

$$\left. \frac{\partial}{\partial i q_0} \Gamma_{R, 1, 1}^{11}(q; q) \right|_{q=0} = 1, \quad (8)$$

$$\left. \frac{\partial}{\partial q_{\perp}^2} \Gamma_{R, 1, 1}^{11}(q; q) \right|_{q=0} = D_R, \quad (9)$$

$$\Gamma_{R, 2, 0}^{11}(q_i = 0) = -2T_R, \quad (10)$$

$$\left. \frac{\partial}{\partial i q_{\parallel}} \Gamma_{R, 1, 2}^{123} \left(-q, \frac{q}{2}, \frac{q}{2} \right) \right|_{q=0} = e_{pR}, \quad (11)$$

$$\Gamma_{R, 1, 3}^{1111}(q_i = 0) = u_{0R}, \quad (12)$$

$$\Gamma_{R, 1, 3}^{1122}(q_i = 0) = u_{1R}. \quad (13)$$

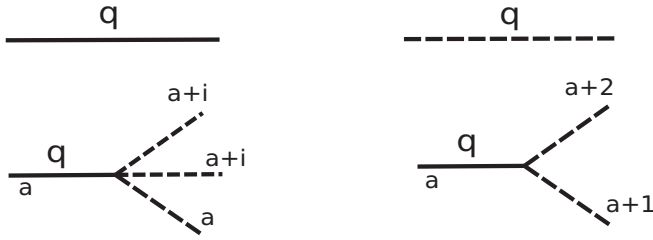


FIG. 1. The straight line represents $G_0(q)$ and the dotted line $C_0(q)$. The four-point vertex takes the value $u_0/6$ if $i = 0$ and $u_1/2$ if $i \neq 0$. The three-point vertex takes the value $iq_{\parallel}e_p$. The dotted branch becomes a straight line when it is hit with an auxiliary field and remains dotted otherwise. We choose the convention that the external ϕ fields hit from the left and the external $\tilde{\phi}$ fields hit from the right. This makes the arrow which is usually attached to the propagator redundant and is hence not explicitly shown.

B. Diagrammatics and perturbative computation

The unperturbed action in Fourier space is

$$S = \sum_a \int_q \tilde{\phi}_a(-q)[-iq_0 + M(\mathbf{q})]\phi_a(q), \quad (14)$$

where $M(\mathbf{q}) = D(\mathbf{q}_{\perp}^2 + \rho q_{\parallel}^2 + r)$ and $\int_q \equiv \frac{1}{(2\pi)^{d+1}} \int d\mathbf{q}_0 d\mathbf{q}$. The Fourier transform of a function $f(x)$ is defined by the relation $f(x) = \int_q f(q)e^{-iq \cdot x}$, where $q \cdot x = q_0 x_0 - \mathbf{q} \cdot \mathbf{x}$. The subscripts \perp , \parallel , and 0 denote the transverse, the longitudinal, and the temporal directions, respectively.

The two nonvanishing unperturbed two-point correlations are

$$\begin{aligned} \langle \phi_a(q_1) \tilde{\phi}_b(q_2) \rangle_0 &= \frac{\delta_{ab} \bar{\delta}(q_1 + q_2)}{-iq_0 + M(\mathbf{q})} = \delta_{ab} \bar{\delta}(q_1 + q_2) G_0(q_1), \\ \langle \phi_a(q_1) \phi_b(q_2) \rangle_0 &= 2T \frac{\delta_{ab} \bar{\delta}(q_1 + q_2)}{q_0^2 + M(\mathbf{q})^2} = \delta_{ab} \bar{\delta}(q_1 + q_2) C_0(q_1), \end{aligned} \quad (15)$$

where $\bar{\delta}(q) \equiv (2\pi)^{d+1} \delta(q)$.

The diagrammatic representations of the two-point Gaussian correlation functions and the perturbations are illustrated in Fig. 1. With the help of these building blocks, we perform the perturbative expansions of the vertex functions to two loops and extract the divergences. This is implemented computationally in the following steps.

(1) For a given vertex function, we obtain all the contributing Feynman diagrams and the corresponding expressions to two loops using the packages FEYNARTS [29] and FEYNCALC [30,31]. For this, we first draw all the topologically distinct irreducible diagrams (topologies) with l external legs that can be constructed with three-point and four-point vertices to two loops, where l is determined by the vertex function we evaluate. Then, we draw all possible realizations of the topologies that can be obtained using the building blocks shown in Fig. 1. Each such realization (Feynman diagram) corresponds to an expression of the form

$$A_f \int_{\{q_i\}} p_{1\parallel} p_{2\parallel} \dots G_0(k_1) G_0(k_2) \dots C_0(k_m) C_0(k_{m+1}) \dots, \quad (16)$$

where $\{q_i\}$ is the set of internal momenta, p_i and k_i are in general linear combinations of the internal and the external momenta, and A_f is the overall factor associated with each diagram.

(2) Derivatives and limits are now applied to isolate the divergences in the expressions obtained in step 1. Integrating out q_{i0} s subsequently leads to an expression of the form

$$B_f \int_{\{q_i\}} \frac{p_{1\parallel}^{m_1} |p_{2\perp}|^{m_2}}{\mathcal{M}_1^{m_1} \mathcal{M}_2^{m_2} \dots} + \text{similar terms}, \quad (17)$$

where \mathcal{M}_i is either $M(\mathbf{k}_i)$ or a sum of $M(\mathbf{k}_i)$ s. The variables p_i and k_i now contain only the internal momenta. Once the parallel components of q_i s are scaled appropriately, $M(\mathbf{k}_i)$ takes the form of the scalar propagator with a factor D .

(3) The integrals obtained by the above procedure are regularized by the method of dimensional regularization and the UV-divergent parts are expanded as

$$\hat{D} \left(\int_{\{q_i\}} \frac{p_{1\parallel}^{m_1} |p_{2\perp}|^{m_2}}{\mathcal{M}_1^{m_1} \mathcal{M}_2^{m_2} \dots} \right) = \frac{\omega_1}{\epsilon^2} + \frac{\omega_2}{\epsilon}, \quad (18)$$

where the operator \hat{D} is defined such that \hat{D} acting on an integral gives the poles of the corresponding dimensionally regularized integral, the parameter $\epsilon = 4 - d$, and ω_1 and ω_2 are real numbers. This step is implemented with the help of the package SECDEC [33–35].

The above steps are elucidated with the help of an example in Appendix A.

(4) Once all the diagrams contributing to a given vertex function are evaluated and the divergences are obtained in negative powers of ϵ , we apply the renormalization conditions with the minimal subtraction scheme to obtain the renormalization constants.

The divergent 1PI Feynman diagrams contributing to the various relevant vertex functions and the renormalization constants are given in Appendices B to I.

There are 11 distinct divergent Feynman diagrams contributing to the various relevant vertex functions at the one-loop order. The presence of both three-point and four-point vertices enhances the number of diagrams at the two-loop order enormously, where the number rises to 319. In the absence of the four-point vertices, the total number of two-loop diagrams reduces to 27, while in the absence of the three-point vertices the total number of two-loop diagrams reduces to 19. For instance, there are 25 two-loop diagrams contributing to $\Gamma_{1,1}^{11}(-q; q)$, as shown in Fig. 4, of which only six diagrams (diagrams 10 to 15) are constructed with three-point vertices alone, while only two diagrams (diagrams 20 and 25) are constructed with four-point vertices alone. Similarly, of the 83 diagrams contributing to $\frac{\partial}{\partial i q_{\parallel}} \Gamma_{1,2}^{123}(-q, \frac{q}{2}, \frac{q}{2})|_{q=0}$, shown in Table X, only 21 diagrams (diagrams 14 to 25 and 73 to 81) are constructed with three-point vertices alone, while none is constructed with four-point vertices alone. Of the 94 diagrams contributing to $\Gamma_{1,3}^{111}(q_i = 0)$, shown in Table XIII, none is constructed with three-point vertices alone, while only eight diagrams (diagrams 47 to 53 and 94) are constructed with four-point

TABLE I. The critical exponents of the NSAPS three-vector model and the standard model [5,22]. For the standard model, the upper critical dimension $\bar{d}_c = 5$, and the exponents are for dimensions $d < \bar{d}_c$. Exp. stands for exponents.

Exp.	NSAPS	Standard model
ν_\perp	$0.5 + 0.192308\epsilon + 0.0955914\epsilon^2$	0.5
ν_\parallel	$0.5 + 0.26923075\epsilon + 0.121763995\epsilon^2$	$1 + \bar{\epsilon}/6$
z_\perp	$2 - 0.0164001\epsilon^2$	4
z_\parallel	$2 - 0.307691\epsilon + 0.044589276\epsilon^2$	$12/(6 + \bar{\epsilon})$
γ_\perp	$1 + 0.384616\epsilon + 0.17021575\epsilon^2$	1
γ_\parallel	$1 + 0.384616\epsilon + 0.17021575\epsilon^2$	$-\bar{\epsilon}/3$
η_\perp^{MS}	$0.0419341\epsilon^2$	0
$\eta_\parallel^{\text{MS}}$	$0.307691\epsilon - 0.019055276\epsilon^2$	$(6 + 2\bar{\epsilon})/(6 + \bar{\epsilon})$
η_\perp^{RS}	$0.1538455\epsilon + 0.03510785\epsilon^2$	$1 + \bar{\epsilon}/3$
$\eta_\parallel^{\text{RS}}$	$-0.1538455\epsilon + 0.072428788\epsilon^2$	$(3 - d)(3 + \bar{\epsilon})/(6 + \bar{\epsilon})$

vertices alone. Of the 116 diagrams contributing to $\Gamma_{1,3}^{1122}(q_i = 0)$, shown in Table XVI, none is constructed with three-point vertices alone and only eight diagrams (diagrams 67 to 73 and 116) are constructed with four-point vertices alone. The only diagram contributing to $\Gamma_{2,0}^{11}(0)$, shown in Table VIII, is constructed with four-point vertices alone.

IV. THE CRITICAL EXPONENTS OF THE NSAPS THREE-VECTOR MODEL

We proceed to write down and solve the RG equation to obtain the scaling form of the vertex functions at the NE fixed point as the temperature approaches the critical value. In particular, we analyze the scaling behavior of the dynamic structure factor and the dynamic susceptibility and extract the exponents associated with them.

For notational simplicity, the subscript R is suppressed in this section, and the following dimensionless couplings are

$$\begin{aligned}
 \beta_0 &= -\epsilon\lambda_0 + 1.5\lambda_0^2 + 3\lambda_1^2 + 0.375\lambda_0\lambda_2 - 1.41667\lambda_0^3 - 6\lambda_1^3 + 0.336482\lambda_2\lambda_0^2 - 2.5\lambda_1^2\lambda_0 + 0.156108\lambda_2^2\lambda_0 \\
 &\quad - 0.341841\lambda_0\lambda_1\lambda_2 - 0.0163937\lambda_1\lambda_2^2 + 0.991439\lambda_1^2\lambda_2, \\
 \beta_1 &= -\epsilon\lambda_1 + 2.5\lambda_1^2 + \lambda_0\lambda_1 + 0.375\lambda_1\lambda_2 - 4.5\lambda_1^3 - 0.0359603\lambda_0^2\lambda_2 - 3\lambda_0\lambda_1^2 + 0.700121\lambda_2\lambda_1^2 - 0.416667\lambda_0^2\lambda_1 \\
 &\quad + 0.158841\lambda_2^2\lambda_1 + 0.135281\lambda_0\lambda_2\lambda_1 - 0.00149424\lambda_0\lambda_2^2, \\
 \beta_2 &= -\epsilon\lambda_2 + 1.125\lambda_2^2 + 3.5\lambda_1\lambda_2 + 0.475028\lambda_2^3 - 0.181794\lambda_0\lambda_2^2 + 1.38638\lambda_1\lambda_2^2 + 0.125\lambda_0^2\lambda_2 - 4.05652\lambda_1^2\lambda_2 \\
 &\quad - 2.90455\lambda_0\lambda_1\lambda_2.
 \end{aligned} \tag{23}$$

Similarly, we obtain Wilson's flow functions by using the renormalization constants given in Appendices B to I together with Eq. (21) and they are explicitly written as

$$\begin{aligned}
 \gamma_\phi &= -0.143841\lambda_0^2 - 0.863046\lambda_1^2, \\
 \gamma_D &= -0.0416667\lambda_0^2 - 0.25\lambda_1^2 - 0.025463\lambda_1\lambda_2, \\
 \gamma_\rho &= -0.75\lambda_2 - 0.0416667\lambda_0^2 - 0.25\lambda_1^2 - 0.312217\lambda_2^2 - 0.308408\lambda_1\lambda_2, \\
 \gamma_T &= -0.0719205\lambda_0^2 - 0.431523\lambda_1^2, \\
 \gamma_r &= -2 + 0.5\lambda_0 + \lambda_1 - 0.25\lambda_0^2 - 1.5\lambda_1^2 + 0.112161\lambda_2\lambda_0 + 0.224321\lambda_1\lambda_2.
 \end{aligned} \tag{24}$$

employed:

$$\begin{aligned}
 \lambda_0 &= \frac{1}{8\pi^2} \frac{T}{D^2 \rho^{1/2}} u_0 \mu^{-\epsilon}, \\
 \lambda_1 &= \frac{1}{8\pi^2} \frac{T}{D^2 \rho^{1/2}} u_1 \mu^{-\epsilon}, \\
 \lambda_2 &= \frac{1}{8\pi^2} \frac{T}{D^3 \rho^{3/2}} e_p^2 \mu^{-\epsilon}.
 \end{aligned} \tag{19}$$

The beta functions are

$$\beta_i = \mu \frac{d\lambda_i}{d\mu}, \tag{20}$$

for $i = 0, 1$, and 2 , and Wilson's flow functions are

$$\begin{aligned}
 \gamma_\phi &= -\mu \frac{\partial}{\partial \mu} \ln Z_\phi, \quad \gamma_{\tilde{\phi}} = -\mu \frac{\partial}{\partial \mu} \ln Z_{\tilde{\phi}}, \quad \gamma_D = \mu \frac{\partial}{\partial \mu} \ln D, \\
 \gamma_\rho &= \mu \frac{\partial}{\partial \mu} \ln \rho, \quad \gamma_T = \mu \frac{\partial}{\partial \mu} \ln T, \quad \gamma_r = \mu \frac{\partial}{\partial \mu} \ln r,
 \end{aligned} \tag{21}$$

where the derivatives are to be taken keeping the bare parameters and couplings constant. Since all the UV divergences can be absorbed into the eight renormalization constants $Z_\phi, Z_D, Z_\rho, Z_T, Z_r, Z_0, Z_1$, and Z_p , the auxiliary field renormalization constant $Z_{\tilde{\phi}}$ is set to unity, which implies that $\gamma_{\tilde{\phi}} = 0$.

We now write down the RG equation, which follows from the fact that the bare vertex functions are independent of μ :

$$\begin{aligned}
 &\left[\mu \frac{\partial}{\partial \mu} + \gamma_\phi \frac{n}{2} + \sum_i \gamma_{s_i} s_i \frac{\partial}{\partial s_i} + \sum_i \beta_i \frac{\partial}{\partial \lambda_i} \right] \\
 &\quad \times \Gamma_{\tilde{n},n}(q_i, s_i, \lambda_i, \mu) = 0,
 \end{aligned} \tag{22}$$

where q_i denotes the external momenta and s_i denotes the elements of the set of parameters $\{D, \rho, T, r\}$.

The beta functions are obtained by using the renormalization constants given in Appendices B to I, in Eqs. (B3), (C1), (D1), (E1), (F1), (G1), (H1), and (I1), together with Eq. (20), and are explicitly written as

The set of equations

$$\beta_i = 0 \quad (25)$$

leads to the critical points. For $\epsilon < 0$, the equilibrium Gaussian fixed point is stable. For $\epsilon > 0$, the following NE fixed point is stable:

$$\begin{aligned} \lambda_0^* &= 0.461538\epsilon + 0.173639\epsilon^2, \\ \lambda_1^* &= 0.153847\epsilon + 0.0837608\epsilon^2, \\ \lambda_2^* &= 0.410255\epsilon - 0.133947\epsilon^2, \end{aligned} \quad (26)$$

where the superscript * denotes the fixed point values of the couplings λ_i . The above result agrees with the one-loop calculations in Ref. [21] to that order. By substituting Eq. (26) in Eq. (24), we further obtain Wilson's flow functions at this fixed point as

$$\begin{aligned} \gamma_D^* &= -0.0164001\epsilon^2, \\ \gamma_\rho^* &= -0.307691\epsilon + 0.0136525\epsilon^2, \\ \gamma_r^* &= -2 + 0.384616\epsilon + 0.117218\epsilon^2, \\ \gamma_T^* &= -0.025534\epsilon^2, \\ \gamma_\phi^* &= -0.051068\epsilon^2. \end{aligned} \quad (27)$$

We now solve the RG equation (22) using the method of characteristics (see, for instance, Ref. [2]). To this end, we define $\mu'(\sigma) = \mu\sigma$, where σ is a dimensionless real parameter, and introduce the running parameters $s'_i(\sigma)$ and the couplings $\lambda'_i(\sigma)$ which respect the following relations:

$$\sigma \frac{ds'_i(\sigma)}{d\sigma} = s'_i(\sigma)\gamma_{s_i}(\sigma), \quad s'_i(1) = s_i, \quad (28)$$

$$\sigma \frac{d\lambda'_i(\sigma)}{d\sigma} = \lambda'_i(\sigma)\beta_i(\sigma), \quad \lambda'_i(1) = \lambda_i. \quad (29)$$

The RG equation (22) together with the above relations yields

$$\begin{aligned} &\Gamma_{\tilde{n},n}(q_i, s_i, \lambda_i, \mu) \\ &= \exp\left(\int_1^\sigma \frac{d\sigma'}{\sigma'} \frac{n}{2} \gamma_\phi(\sigma')\right) \Gamma_{\tilde{n},n}(q_i, s'_i(\sigma), \lambda'_i(\sigma), \mu\sigma). \end{aligned} \quad (30)$$

At the fixed points, the solution to Eq. (28) gives simple power-law behavior, and at the NE fixed point we obtain

$$s'_i(\sigma) \approx s_i \sigma^{\gamma_{s_i}^*}. \quad (31)$$

Using the above result in Eq. (30), we obtain the critical scaling form of the vertex functions at the NE fixed point:

$$\Gamma_{\tilde{n},n}(q_i, s_i, \mu) = \sigma^{\frac{n}{2}\gamma_\phi^*} \Gamma_{\tilde{n},n}(q_i, s_i \sigma^{\gamma_{s_i}^*}, \mu\sigma), \quad (32)$$

where we have not shown the arguments of Γ which are not affected by rescaling. In the limit $r \rightarrow 0$, the parameter σ scales as $\sigma \propto r^{-1/\gamma_r^*}$, as can be seen from Eq. (31).

From Eq. (32) the scaling forms of the dynamic structure factor $S(\mathbf{q}, t) = \int_{q_0} e^{-iq_0 t} \Gamma_{2,0}(q)/|\Gamma_{1,1}(q)|^2$ and the dynamic susceptibility $\chi(q) = 1/\Gamma_{1,1}(q)$ follow as

$$\begin{aligned} &S(\mathbf{q}_\perp, q_\parallel, t, r) \\ &= \sigma^{-2+\gamma_r^*-\gamma_\phi^*-\gamma_D^*} S\left(\frac{\mathbf{q}_\perp}{\sigma}, \frac{q_\parallel}{\sigma^{1-\gamma_\rho^*/2}}, t\sigma^{2+\gamma_D^*}, \frac{r}{\sigma^{-\gamma_r^*}}\right), \end{aligned} \quad (33)$$

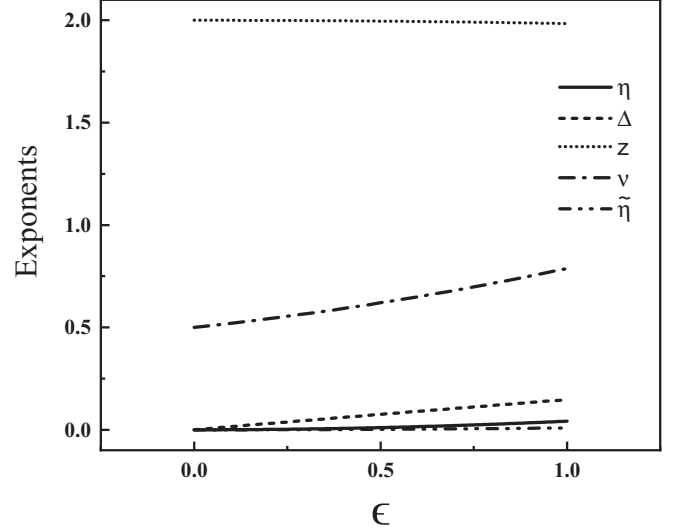


FIG. 2. The independent exponents of the NSAPS three-vector model as a function of ϵ .

$$\begin{aligned} &\chi(\mathbf{q}_\perp, q_\parallel, t, r) \\ &= \sigma^{-2-\gamma_\phi^*/2-\gamma_D^*} \chi\left(\frac{\mathbf{q}_\perp}{\sigma}, \frac{q_\parallel}{\sigma^{1-\gamma_\rho^*/2}}, t\sigma^{2+\gamma_D^*}, \frac{r}{\sigma^{-\gamma_r^*}}\right). \end{aligned} \quad (34)$$

Comparing Eqs. (33) and (34) with the standard scaling forms [5],

$$S(\mathbf{q}_\perp, q_\parallel, t, r) = \sigma^{-2+\eta} S\left(\frac{\mathbf{q}_\perp}{\sigma}, \frac{q_\parallel}{\sigma^{1+\Delta}}, t\sigma^z, \frac{r}{\sigma^{1/\nu}}\right), \quad (35)$$

$$\chi(\mathbf{q}_\perp, q_\parallel, t, r) = \sigma^{-z+\tilde{\eta}/2+\eta/2} \chi\left(\frac{\mathbf{q}_\perp}{\sigma}, \frac{q_\parallel}{\sigma^{1+\Delta}}, \frac{q_0}{\sigma^z}, \frac{r}{\sigma^{1/\nu}}\right), \quad (36)$$

we obtain the exponents

$$\begin{aligned} \eta &= \gamma_T^* - \gamma_D^* - \gamma_\phi^* = 0.0419341\epsilon^2, \\ \Delta &= -\gamma_\rho^*/2 = 0.1538455\epsilon - 0.00682625\epsilon^2, \\ z &= 2 + \gamma_D^* = 2 - 0.0164001\epsilon^2, \\ \nu &= -1/\gamma_r^* = 0.5 + 0.192308\epsilon + 0.0955914\epsilon^2, \\ \tilde{\eta} &= \gamma_D^* - \gamma_T^* = 0.0091339\epsilon^2, \end{aligned} \quad (37)$$

which are correct to second order in ϵ . A graph showing the behavior of these exponents as a function of ϵ is given in Fig. 2. As ϵ increases the exponents are, of course, expected to deviate from the exact values significantly.

The other standard anisotropy exponents [5] can be written in terms of the above five exponents. The transverse and the longitudinal dynamic exponents are

$$z_\perp = z, \quad z_\parallel = z/(1 + \Delta). \quad (38)$$

The significance of these exponents can be realized by considering the scaling form of the dynamic structure factor given in Eq. (35). Choosing the parameter $\sigma = t^{-1/z}$ and substituting in Eq. (35) yields

$$S(\mathbf{q}_\perp, q_\parallel, t) = f(\mathbf{q}_\perp t^{1/z_\perp}, q_\parallel t^{1/z_\parallel}). \quad (39)$$

This implies that the transverse length scale behaves with time as $\langle l_\perp \rangle \propto t^{1/z_\perp}$. Using Eqs. (37) and (38) we obtain

explicitly $1/z_{\perp} = 1/2 + 0.00410003\epsilon^2$. Clearly, the higher order correction to the the dynamic exponent z shows that the spread of fluctuations in the transverse direction is superdiffusive. This is a contrasting feature when compared to the familiar $O(n)$ -symmetric model A. There the dynamic exponent $z = 2 + 0.363046(n+2)\epsilon^2/(n+8)^2$ or $1/z = 1/2 - 0.0907615(n+2)\epsilon^2/(n+8)^2$, where n is the number of field components [10], indicating a subdiffusive spread of fluctuations.

Again, from Eq. (39), we deduce that the longitudinal length scale behaves with time as $\langle l_{\parallel} \rangle \propto t^{1/z_{\parallel}}$. Using Eqs. (37) and (38) we infer that fluctuations spread superdiffusively in the longitudinal direction too. However, it spreads faster in this direction than in the transverse direction as $z_{\parallel} < z_{\perp}$. This speeding up of fluctuations in the direction of the bias is also observed in several of the conserved models with strong anisotropy [5,19,22,36]. For instance, in the case of the so-called standard model [5], $z_{\perp} = 4$ and $z_{\parallel} = 12/(6 + \bar{\epsilon})$, where $\bar{\epsilon} = 5 - d$. Clearly, $z_{\parallel} < z_{\perp}$, indicating that fluctuations decay faster in the longitudinal direction than in the transverse direction. A comparison of the critical exponents of the NSAPS three-vector model to those of the standard model is given in Table I.

Unlike the standard model, and the other strongly anisotropic conserved models [5,19,22,36], where the spread of fluctuations is superdiffusive in the longitudinal direction and subdiffusive in the transverse direction, here, it is superdiffusive in the transverse as well as the longitudinal directions.

We now discuss the correlation length exponents. The transverse correlation length exponent $\nu_{\perp} = \nu$, while the longitudinal correlation length exponent $\nu_{\parallel} = \nu(1 + \Delta)$. As the strong anisotropy exponent $\Delta > 0$, $\nu_{\parallel} > \nu_{\perp}$. This implies that the longitudinal correlation length diverges faster than the transverse correlation length as the temperature approaches the critical value. As a result, near the critical point, correlations extend over a larger length scale in the longitudinal direction than in the transverse direction. The analogous conserved models also exhibit this feature. For the standard model, $\nu_{\perp} = 1/2$ and $\nu_{\parallel} = 1 + \bar{\epsilon}/6$ [5,22]. Clearly, $\nu_{\parallel} > \nu_{\perp}$, implying the feature in question.

There are four η -like exponents, two in the momentum space, and two in the real space. The two momentum space η -like exponents, $\eta_{\perp}^{\text{MS}} = \eta$ and $\eta_{\parallel}^{\text{MS}} = (\eta + 2\Delta)/(1 + \Delta)$, determine the anisotropic power-law behavior of the dynamic structure factor in momentum space and the two real space η -like exponents, $\eta_{\perp}^{\text{RS}} = \eta + \Delta$ and $\eta_{\parallel}^{\text{RS}} = (\eta - \Delta)/(1 + \Delta)$, determine the anisotropic power-law behavior of the dynamic structure factor in real space. The values of these exponents, obtained by substituting Eq. (37) in the above relations, are given in Table I.

The significance of the η -like exponents can be realized by considering the momentum space dynamic structure factor at two different limits, restricting to the case of $t = 0$ for convenience. From Eq. (35) we deduce that the transverse and the longitudinal structure factors scale as

$$S_{\perp} \equiv S(\mathbf{q}_{\perp} \rightarrow 0, q_{\parallel} = 0) \sim |\mathbf{q}_{\perp}|^{-2+\eta_{\perp}^{\text{MS}}},$$

$$S_{\parallel} \equiv S(\mathbf{q}_{\perp} = 0, q_{\parallel} \rightarrow 0) \sim q_{\parallel}^{-2+\eta_{\parallel}^{\text{MS}}}. \quad (40)$$

From the values given in Table I we observe that $\eta_{\parallel}^{\text{MS}} > \eta_{\perp}^{\text{MS}}$, implying that near the critical point the longitudinal structure factor is less dominant than the transverse one in the long wavelength limit. This is also the case with the standard model [5,22]. For model A and other isotropic models there is, of course, no distinction between the transverse and the longitudinal ones.

Unlike equilibrium models, here the scaling behavior of the susceptibility cannot be extracted from the structure factor [5]. The transverse and the longitudinal susceptibilities scale as $\chi_{\perp} \sim r^{-\gamma_{\perp}}$ and $\chi_{\parallel} \sim r^{-\gamma_{\parallel}}$, where $\chi_{\perp} \equiv \chi(\mathbf{q}_{\perp} \rightarrow 0, q_{\parallel} = 0)$ and $\chi_{\parallel} \equiv \chi(\mathbf{q}_{\perp} = 0, q_{\parallel} \rightarrow 0)$. From Eq. (36) we obtain

$$\gamma_{\perp} = \gamma_{\parallel} = \nu(z - \tilde{\eta}/2 - \eta/2). \quad (41)$$

As opposed to the strongly anisotropic models that follow conserving dynamics, the susceptibility exponents γ_{\perp} and γ_{\parallel} are equal [5,19,22,36].

To summarize, we studied the critical scaling behavior of the NSAPS three-vector model, which belongs to a new genuine nonequilibrium universality class. We obtained the critical exponents, which characterize the anisotropic power-law behavior of the dynamic structure factor and the dynamic susceptibility, to two-loop order. Among them is the important strong anisotropy exponent Δ that captures the effects of the spatially biased drive. We briefly mentioned the similarities and the dissimilarity in the critical behavior of the model to that of strongly anisotropic models that follow conserving dynamics.

ACKNOWLEDGMENT

I extend my sincere gratitude to Sreedhar B. Dutta, who suggested this problem and has spent hours engaging in fruitful discussions during the progress of the work and the preparation of the paper.

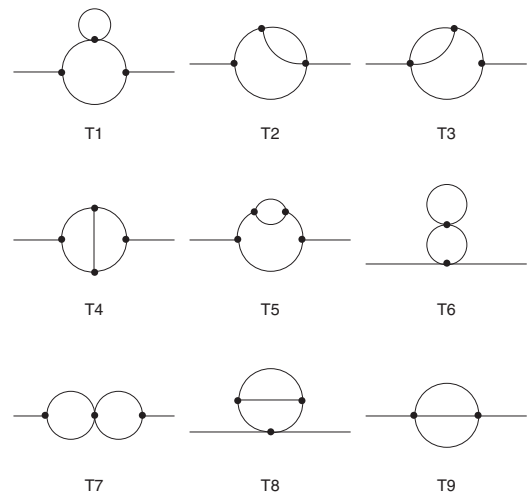


FIG. 3. All possible irreducible two-loop topologies with two external lines constructible with three-point and four-point vertices.

APPENDIX A: GENERATING AND EVALUATING FEYNMAN DIAGRAMS: AN EXAMPLE

To obtain the Feynman diagrams that contribute to a vertex function, we first draw all the relevant topologies. For instance, to obtain the two-loop Feynman diagrams contributing to $\Gamma_{1,1}^{11}$, we draw all the distinct irreducible two-loop topologies with two external legs that can be constructed with three-point and four-point vertices, as shown in Fig. 3. Any two-loop contribution to $\Gamma_{1,1}^{11}$ must be topologically similar to one of these diagrams. Now, we use the building blocks shown in Fig. 1 to construct all the possible realizations of these topologies. This leads to the Feynman diagrams shown in Fig. 4.

Each of the diagrams in Fig. 4 corresponds to an expression that is of the form given in Eq. (25). For instance, diagram 22 corresponds to

$$\mathcal{I}_{22} = 12T^2 u_0 e_p^2 \int_{q_1, q_2} (q_{1\parallel} + q_{2\parallel}) q_{2\parallel} C_0(q_1) C_0(q_1 + q_2) G_0(-q_1 - q_2) G_0(-q_2).$$

All the above steps were implemented in MATHEMATICA [32] with the help of FEYNALCALC [30,31] and FEYNARTS [29].

We can now proceed to extract the divergences. For instance, setting the external momenta to zero we obtain the quadratically divergent part which renormalizes the mass parameter r . The above integral does not depend on the external momenta and remains unchanged. Integrating out q_{10} and q_{20} from the above integral and making the transformation, $\{q_{i\perp}, \sqrt{\rho}q_{i\parallel}\} \rightarrow \{\sqrt{r}q_{i\perp}, \sqrt{r}q_{i\parallel}\}$, we obtain

$$\mathcal{I}_{22} = \frac{3}{2} \frac{T^2 u_0 e_p^2}{D^4 \rho^2} r^{d-3} \int_{q_1, q_2} \frac{(q_{1\parallel} + q_{2\parallel}) q_{2\parallel}}{N(q_1) N(q_1 + q_2)^2 [N(q_1) + N(q_2) + N(q_1 + q_2)]} \tag{A1}$$

where $N(q) = q^2 + 1$. The UV-divergent parts of the above integral are expanded in powers of $\frac{1}{\epsilon}$ by employing the dimensional regularization scheme with the help of the package SECDEC [33–35]:

$$\widehat{\mathcal{D}} \left(\int_{q_1, q_2} \frac{q_{1\parallel} q_{2\parallel}}{N(q_1) N(q_1 + q_2)^2 [N(q_1) + N(q_2) + N(q_1 + q_2)]} \right) = \frac{1}{256\pi^4} \left(\frac{0.125}{\epsilon^2} - \frac{0.563592}{\epsilon} \right)$$

and

$$\widehat{\mathcal{D}} \left(\int_{q_1, q_2} \frac{q_{2\parallel}^2}{N(q_1) N(q_1 + q_2)^2 [N(q_1) + N(q_2) + N(q_1 + q_2)]} \right) = \frac{1}{256\pi^4} \left(-\frac{0.75}{\epsilon^2} + \frac{0.290792}{\epsilon} \right). \tag{A2}$$

Equation (A1) together with Eq. (A2) gives the UV-divergent parts of diagram 22:

$$\widehat{\mathcal{D}}(\mathcal{I}_{22}) = -\frac{3}{512\pi^4} \frac{T^2 u_0 e_p^2}{D^4 \rho^2} r^{d-3} \left(\frac{0.625}{\epsilon^2} + \frac{0.2728}{\epsilon} \right). \tag{A3}$$

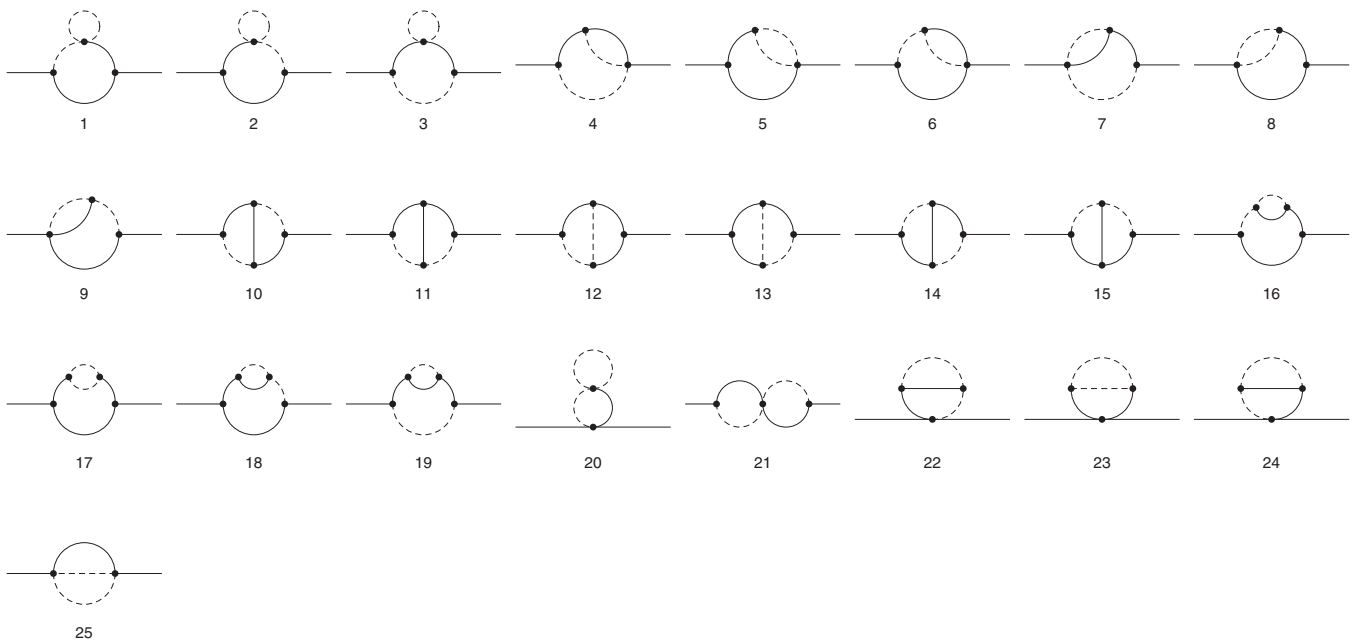



FIG. 4. Two-loop Feynman diagrams contributing to $\Gamma_{1,1}^{11}(q)$.

TABLE II. One-loop contribution to $\Gamma_{1,1}^{11}(0)$.

Diagrams	Divergence in ϵ -expansion
	$D r^{1-\epsilon/2} \left(\frac{g_0}{2} + g_1 \right) \frac{1}{\epsilon}$

APPENDIX B: $\Gamma_{1,1}^{11}(0)$

Table II shows the only one-loop diagram contributing to $\Gamma_{1,1}^{11}(0)$ and its divergent contribution. The divergent parts of the two-loop diagrams contributing to $\Gamma_{1,1}^{11}(0)$ have the general form

$$\widehat{D}(\mathcal{I}(q=0)) = r^{1-\epsilon} D \mathcal{A} \left(\frac{n}{\epsilon} + \frac{m}{\epsilon^2} \right) \tag{B1}$$

where \mathcal{I} is the integral that a diagram represents and n and m are real numbers. The factor \mathcal{A} is a function of the modified couplings

$$g_0 \equiv \frac{T}{8\pi^2 D^2 \rho^{1/2}} u_0, \quad g_1 \equiv \frac{T}{8\pi^2 D^2 \rho^{1/2}} u_1, \quad \text{and } g_2 \equiv \frac{T}{8\pi^2 D^3 \rho^{3/2}} e_p^2. \tag{B2}$$

Table III shows the two-loop diagrams and their respective contributions.

Collecting the divergences from all the diagrams shown in Tables II and III and applying the renormalization condition (6) we obtain the renormalization constant Z_r . In terms of the dimensionless renormalized couplings λ_i , which are defined in Eq. (19), Z_r can be written explicitly as

$$\begin{aligned} Z_r = 1 + & \frac{1}{\epsilon} (\lambda_1 + 0.5\lambda_0 - 0.125\lambda_0^2 - 0.75\lambda_1^2 + 0.0560803\lambda_0\lambda_2 + 0.112161\lambda_1\lambda_2) \\ & + \frac{1}{\epsilon^2} (0.5\lambda_0^2 + 2.5\lambda_1^2 + \lambda_0\lambda_1 + 0.09375\lambda_0\lambda_2 + 0.1875\lambda_1\lambda_2). \end{aligned} \tag{B3}$$

APPENDIX C: $\frac{\partial}{\partial q_i^2} \Gamma_{1,1}^{11}(q)|_{q=0}$

Table IV shows the only one-loop diagram contributing to $\frac{\partial}{\partial q_i^2} \Gamma_{1,1}^{11}(q)|_{q=0}$ and its divergent contribution.

The divergent parts of the two-loop diagrams contributing to $\frac{\partial}{\partial q_i^2} \Gamma_{1,1}^{11}(q)|_{q=0}$ have the general form $r^{-\epsilon} D \rho \mathcal{A} \left(\frac{n}{\epsilon} + \frac{m}{\epsilon^2} \right)$. Table VII shows these diagrams and their respective divergences. Collecting the divergences from all the diagrams given in Tables IV

TABLE III. Two-loop contributions to $\Gamma_{1,1}^{11}(0)$.

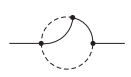

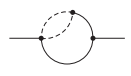
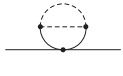
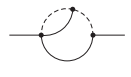
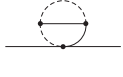

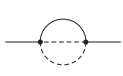

Diagram	\mathcal{A}, n, m	Diagram	\mathcal{A}, n, m
	$g_1 g_2, -0.1364, -0.3125$		$(g_0 + 2g_1) g_2, -0.0341, -0.078125$
	$g_1 g_2, -0.133328, -0.125$		$(g_0 + 2g_1) g_2, 0.0846443, 0.0625$
	$g_1 g_2, 0.269728, 0.4375$		$(g_0 + 2g_1) g_2, -0.0341, -0.078125$
	$(g_0 + 2g_1)^2, 0.0193039, -0.25$		$g_0^2 + 6g_1^2, -0.230696, -0.25$

TABLE IV. One-loop contribution to $\frac{\partial}{\partial q_{\parallel}^2} \Gamma_{1,1}^{11}(q)|_{q=0}$.

Diagrams	Divergence in ϵ -expansion
	$-r^{-\epsilon/2} D\rho g_2 \left(\frac{0.75}{\epsilon}\right)$

and VII and applying the renormalization condition (7) yields


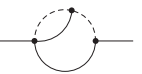

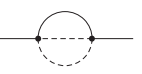
$$Z_{\rho} = 1 + \frac{1}{\epsilon} (-0.75\lambda_2 - 0.0208333\lambda_0^2 - 0.125\lambda_1^2 - 0.156109\lambda_2^2 - 0.154204\lambda_1\lambda_2) + \frac{1}{\epsilon^2} (-0.140625\lambda_2^2 - 1.3125\lambda_1\lambda_2). \tag{C1}$$

APPENDIX D: $\frac{\partial}{\partial i q_0} \Gamma_{1,1}(q)|_{q=0}$

There is no one-loop contribution to $\frac{\partial}{\partial i q_0} \Gamma_{1,1}(q)|_{q=0}$. The divergent parts of the two-loop diagrams have the general form $r^{-\epsilon} \mathcal{A}(\frac{n}{\epsilon} + \frac{m}{\epsilon^2})$. Table V shows these diagrams and their respective divergences. Collecting the divergences from all the diagrams given in Table V and applying the renormalization condition (8) yields

$$Z = 1 + \frac{1}{\epsilon} (-0.0359603\lambda_0^2 - 0.215762\lambda_1^2). \tag{D1}$$

TABLE V. Two-loop contributions to $\frac{\partial}{\partial i q_0} \Gamma_{1,1}(q)|_{q=0}$.

Diagram	\mathcal{A}, n, m	Diagram	\mathcal{A}, n, m
	$g_1 g_2, 0.0172122, -0.0468752$		$g_1 g_2, -0.00208572, 0.0468752$
	$g_1 g_2, -0.01512692, 0$		$g_0^2 + 6g_1^2, -0.03596025, 0$

APPENDIX E: $\frac{\partial}{\partial q_{\perp}^2} \Gamma_{1,1}^{11}(q)|_{q=0}$

There is no one-loop contribution to $\frac{\partial}{\partial q_{\perp}^2} \Gamma_{1,1}^{11}(q)|_{q=0}$. The divergent parts of the two-loop diagrams have the general form $r^{-\epsilon} D\mathcal{A}(\frac{n}{\epsilon} + \frac{m}{\epsilon^2})$. Table VI shows these diagrams and their respective divergences. Collecting the divergences from all the diagrams given in Table VI and applying the renormalization condition (9) yields

$$Z_D = 1 + \frac{1}{\epsilon} (-0.0208333\lambda_0^2 - 0.125\lambda_1^2 - 0.0127315\lambda_1\lambda_2). \tag{E1}$$

TABLE VI. Two-loop contributions to $\frac{\partial}{\partial q_{\perp}^2} \Gamma_{1,1}^{11}(q)|_{q=0}$.




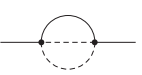

Diagram	\mathcal{A}, n, m	Diagram	\mathcal{A}, n, m
	$g_1 g_2, -0.00224807, -0.03125$		$g_1 g_2, -0.0000398716, 0.03125$
	$g_1 g_2, -0.01044354, 0$		$g_0^2 + 6g_1^2, -0.0208333, 0$

TABLE VII. Two-loop contributions to $\frac{\partial}{\partial q_0^2} \Gamma_{1,1}^{11}(q)|_{q=0}$.

Diagram	\mathcal{A}, n, m	Diagram	\mathcal{A}, n, m
	$g_0 g_2 + 2g_1 g_2, -0.0520833, 0$		$g_2^2, -0.00835706, 0.0234375$
	$g_0 g_2 + 2g_1 g_2, -0.09375, 0$		$g_2^2, 0.0020853, -0.046875$
	$g_0 g_2 + 2g_1 g_2, -0.0416667, 0$		$g_2^2, -0.0180942, 0.0234375$
	$g_1 g_2, -0.306357, 0.375$		$g_2^2, 0.018626, -0.0117188$
	$g_1 g_2, 0.143841, 0$		$g_2^2, -0.0401051, 0.0234375$
	$g_1 g_2, 0.0875039, -0.09375$		$g_2^2, -0.0283968, 0$
	$g_1 g_2, -0.216176, 0.1875$		$g_2^2, -0.0580853, 0.0234375$
	$g_1 g_2, -0.0313306, 0$		$g_2^2, -0.0794423, 0.09375$
	$g_1 g_2, -0.000119615, 0.09375$		$g_1 g_2, -0.370412, 0.75$
	$g_2^2, -0.0180942, 0.0234375$		$g_0^2 + 6g_1^2, -0.0208333, 0$
	$g_2^2, 0.0160218, -0.0117188$	-	-

TABLE VIII. Two-loop contribution to $\Gamma_{2,0}^{11}(q)|_{q=0}$.

Diagram	Divergence
	$r^{-\epsilon} T \left(\frac{g_0^2}{6} + g_1^2 \right) \left(\frac{0.4315235}{\epsilon} \right)$

APPENDIX F: $\Gamma_{2,0}^{11}(q)|_{q=0}$

There is no one-loop contribution to $\Gamma_{2,0}^{11}(q)|_{q=0}$. The only two-loop contribution is given in Table VIII. Collecting the divergence from the diagram given in Table VIII and applying the renormalization condition (10) yields

$$Z_T = 1 + \frac{1}{\epsilon} (-0.0359603\lambda_0^2 - 0.215762\lambda_1^2). \tag{F1}$$

APPENDIX G: $\frac{\partial}{\partial i q_{\parallel}} \Gamma^{123}_{1,2}(-q, \frac{q}{2}, \frac{q}{2})|_{q=0}$

Table IX shows the one-loop diagrams contributing to $\frac{\partial}{\partial i q_{\parallel}} \Gamma^{123}_{1,2}(-q, \frac{q}{2}, \frac{q}{2})|_{q=0}$ and their respective divergent contributions. The divergent parts of the one-loop diagrams have the general form $r^{-\epsilon/2} e_p \mathcal{A}(\frac{n}{\epsilon})$.

As the first and the second diagrams in Table IX cancel each other there is no g_2 contribution to the renormalization constant Z_p at the one-loop order.

Table X shows the two-loop diagrams contributing to $\frac{\partial}{\partial i q_{\parallel}} \Gamma^{123}_{1,2}(-q, \frac{q}{2}, \frac{q}{2})|_{q=0}$.

The divergent contributions of the above diagrams to $\frac{\partial}{\partial i q_{\parallel}} \Gamma^{123}_{1,2}(-q, \frac{q}{2}, \frac{q}{2})|_{q=0}$ have the general form, $r^{-\epsilon} e_p \mathcal{A}(\frac{n}{\epsilon} + \frac{m}{\epsilon^2})$. The parameters \mathcal{A} , n , and m for each of the above diagrams are listed against their respective diagram numbers in Table XI.

Collecting the divergences from all the diagrams given in Tables IX and X and applying the renormalization condition (11) yields

$$Z_p = 1 + \frac{1}{\epsilon} (1.75\lambda_1 - 1.20163\lambda_1^2 + 0.00167566\lambda_2^2 - 0.726138\lambda_0\lambda_1 + 0.221394\lambda_1\lambda_2 - 0.0454484\lambda_0\lambda_2) + \frac{1}{\epsilon^2} (3.71875\lambda_1^2 + 0.875\lambda_0\lambda_1 + 0.328125\lambda_1\lambda_2). \tag{G1}$$

TABLE IX. One-loop contributions to $\frac{\partial}{\partial i q_{\parallel}} \Gamma^{123}_{1,2}(-q, \frac{q}{2}, \frac{q}{2})|_{q=0}$.

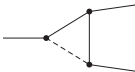
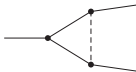
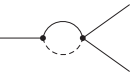
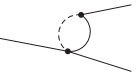
Diagram	\mathcal{A}, n	Diagram	\mathcal{A}, n	Diagram	\mathcal{A}, n	Diagram	\mathcal{A}, n
	$g_2, 0.125$		$g_2, -0.125$		$g_1, 1$		$g_1, 0.75$

TABLE X. Two-loop contributions to $\frac{\partial}{\partial i q_{\parallel}} \Gamma^{123}_{1,2}(-q, \frac{q}{2}, \frac{q}{2})|_{q=0}$.

The table contains 83 Feynman diagrams, numbered 1 through 83, arranged in a grid. The first nine rows contain 8 diagrams each, and the tenth row contains 3 diagrams. Each diagram represents a two-loop contribution to the function $\frac{\partial}{\partial i q_{\parallel}} \Gamma^{123}_{1,2}(-q, \frac{q}{2}, \frac{q}{2})|_{q=0}$. The diagrams are drawn with solid and dashed lines, representing different types of propagators and interactions. Some diagrams include vertices and external lines, while others are more complex loop structures.

TABLE XI. Divergent contributions of the diagrams shown in Table X.

No.	\mathcal{A}	n	m
1	$(g_0 + 2g_1)g_2$	-0.00899006	0
2	$(g_0 + 2g_1)g_2$	-0.0132699	0
3	$(g_0 + 2g_1)g_2$	-0.0359603	0
4	$(g_0 + 2g_1)g_2$	0.0201779	-0.03125
5	$(g_0 + 2g_1)g_2$	0.00427981	0
6	$(g_0 + 2g_1)g_2$	0.0206083	-0.03125
7	$(g_0 + 2g_1)g_2$	0.0359603	0
8	$(g_0 + 2g_1)g_2$	-0.0540561	0.0625
9	$(g_0 + 2g_1)g_2$	0.0125967	-0.0117188
10	$(g_0 + 2g_1)g_2$	0.000396799	-0.0117188
11	$(g_0 + 2g_1)g_2$	-0.0297559	0.0117188
12	$(g_0 + 2g_1)g_2$	0.00759028	-0.0117188
13	$(g_0 + 2g_1)g_2$	-0.00502626	0.0234375
14	g_2^2	0.00328934	-0.00390625
15	g_2^2	-0.0160106	0.015625
16	g_2^2	-0.00344199	0
17	g_2^2	-0.000192796	0.0078125
18	g_2^2	0.00208366	-0.0078125
19	g_2^2	0.0137743	-0.0117188
20	g_2^2	-0.0216832	0.015625
21	g_2^2	0.00586539	-0.0078125
22	g_2^2	0.0123075	0
23	g_2^2	-0.000657054	0.0078125
24	g_2^2	-0.0160893	0
25	g_2^2	0.019079	-0.015625
26	$g_1(2g_0 + 3g_1)$	0.127185	-0.25
27	$g_1(2g_0 + 3g_1)$	-0.107881	0
28	$g_1(g_0 + 2g_1)$	-0.00449503	0
29	$g_1(g_0 + 2g_1)$	-0.00449503	0
30	$g_1(2g_0 + 3g_1)$	-0.0492301	0
31	$g_1(2g_0 + 3g_1)$	0.089859	-0.09375
32	$g_1(2g_0 + 3g_1)$	-0.0398513	-0.09375
33	g_1^2	0.0302539	0
34	g_1^2	0.209432	-0.28125
35	g_1^2	0.00417054	-0.09375
36	$g_1(g_0 + 2g_1)$	-0.0230808	0
37	$g_1(g_0 + 2g_1)$	0.09375	0
38	$g_1(g_0 + 2g_1)$	0.0520833	0
39	g_1^2	0.306357	-0.375
40	g_1^2	-0.143841	0
41	g_1^2	-0.0875039	0.09375
42	$(g_0 + 2g_1)g_2$	-0.03125	0
43	$(g_0 + 2g_1)g_2$	0.015625	0
44	$(g_0 + 2g_1)g_2$	0.015625	0
45	g_1g_2	0.103402	-0.125
46	g_1g_2	-0.103402	0.125
47	g_1g_2	-0.0901321	0.125
48	g_1g_2	0.0719206	0
49	g_1g_2	0.0875039	-0.09375
50	g_1g_2	0.126092	-0.125
51	g_1g_2	-0.0719206	0
52	g_1g_2	-0.0609641	0.09375
53	g_1g_2	0.0875039	-0.09375
54	g_1g_2	0.0719206	0
55	g_1g_2	0.0609641	-0.09375
56	g_1g_2	0.0201779	-0.03125

TABLE XI. (Continued.)

No.	\mathcal{A}	n	m
57	$g_1 g_2$	0.00690802	-0.03125
58	$g_1 g_2$	-0.0132699	0
59	$g_1 g_2$	-0.0138161	0.0625
60	$g_1 g_2$	0.0854314	-0.0820313
61	$g_1 g_2$	-0.0333353	0.046875
62	$g_1 g_2$	-0.0121528	0
63	$g_1 g_2$	-0.0115466	0.0351563
64	$g_1 g_2$	0.105484	-0.09375
65	$g_1 g_2$	0.00600193	-0.0234375
66	$g_1 g_2$	0.0283968	0
67	$g_1 g_2$	0.0140635	-0.0234375
68	$g_1 g_2$	0.0361885	-0.046875
69	$g_1 g_2$	-0.0160218	0.0117188
70	$g_1 g_2$	-0.00208526	0.046875
71	$g_1 g_2$	0.0135654	-0.0234375
72	$g_1 g_2$	-0.018626	0.0117187
73	g_2^2	0.00806154	0
74	g_2^2	-0.00471026	0
75	g_2^2	0.00378175	0
76	g_2^2	-0.00378175	0
77	g_2^2	0.0445327	-0.0351563
78	g_2^2	0.0217619	0
79	g_2^2	0.0274811	-0.0351563
80	g_2^2	-0.0757955	0.0703125
81	g_2^2	-0.0179801	0
82	g_1^2	0.577216	-1
83	g_1^2	0.370412	-0.75

APPENDIX H: $\Gamma_{1,3}^{1111}(0)$

Table XII shows the one-loop diagrams contributing to $\Gamma_{1,3}^{1111}(0)$ and their respective divergent contributions. The divergent part of the one-loop diagrams have the general form $r^{-\epsilon/2} u_0 \mathcal{A}(\frac{n}{\epsilon})$.

As the first two diagrams in Table XII cancel each other there is no g_2 contribution to the renormalization constant Z_0 at the one-loop order. Table XIII shows the two-loop diagrams contributing to $\Gamma_{1,3}^{1111}(0)$.

The divergent contributions of the above diagrams to $\Gamma_{1,3}^{1111}(0)$ have the general form $r^{-\epsilon} u_0 \mathcal{A}(\frac{n}{\epsilon} + \frac{m}{\epsilon^2})$. The parameters \mathcal{A} , n , and m for each of the above diagrams are listed against their respective diagram numbers in Table XIV.

Collecting the divergences from all the diagrams given in Tables XII and XIII and applying the renormalization condition (12) yields

$$\begin{aligned}
 Z_0 = & 1 + \frac{1}{\epsilon} \left(1.5\lambda_0 - 0.75\lambda_0^2 - 1.5\lambda_1^2 - 0.26712\lambda_1\lambda_2 + 0.168241\lambda_0\lambda_2 - \frac{3\lambda_1^3}{\lambda_0} + \frac{0.49572\lambda_2\lambda_1^2}{\lambda_0} + \frac{3\lambda_1^2}{\lambda_0} - \frac{0.00819685\lambda_2^2\lambda_1}{\lambda_0} \right) \\
 & + \frac{1}{\epsilon^2} \left(2.25\lambda_0^2 + 7.5\lambda_1^2 - 0.28125\lambda_0\lambda_2 + \frac{7.5\lambda_1^3}{\lambda_0} + \frac{0.5625\lambda_2\lambda_1^2}{\lambda_0} \right). \tag{H1}
 \end{aligned}$$

TABLE XII. One-loop contributions to $\Gamma_{1,3}^{1111}(0)$.

Diagram	\mathcal{A}, n	Diagram	\mathcal{A}, n	Diagram	\mathcal{A}, n
	$\frac{g_1 g_2}{g_0}, 0.75$		$\frac{g_1 g_2}{g_0}, -0.75$		$g_0 + \frac{2g_1^2}{g_0}, 1.5$

TABLE XIII. Two-loop diagrams contributing to $\Gamma_{1,3}^{111}(0)$.

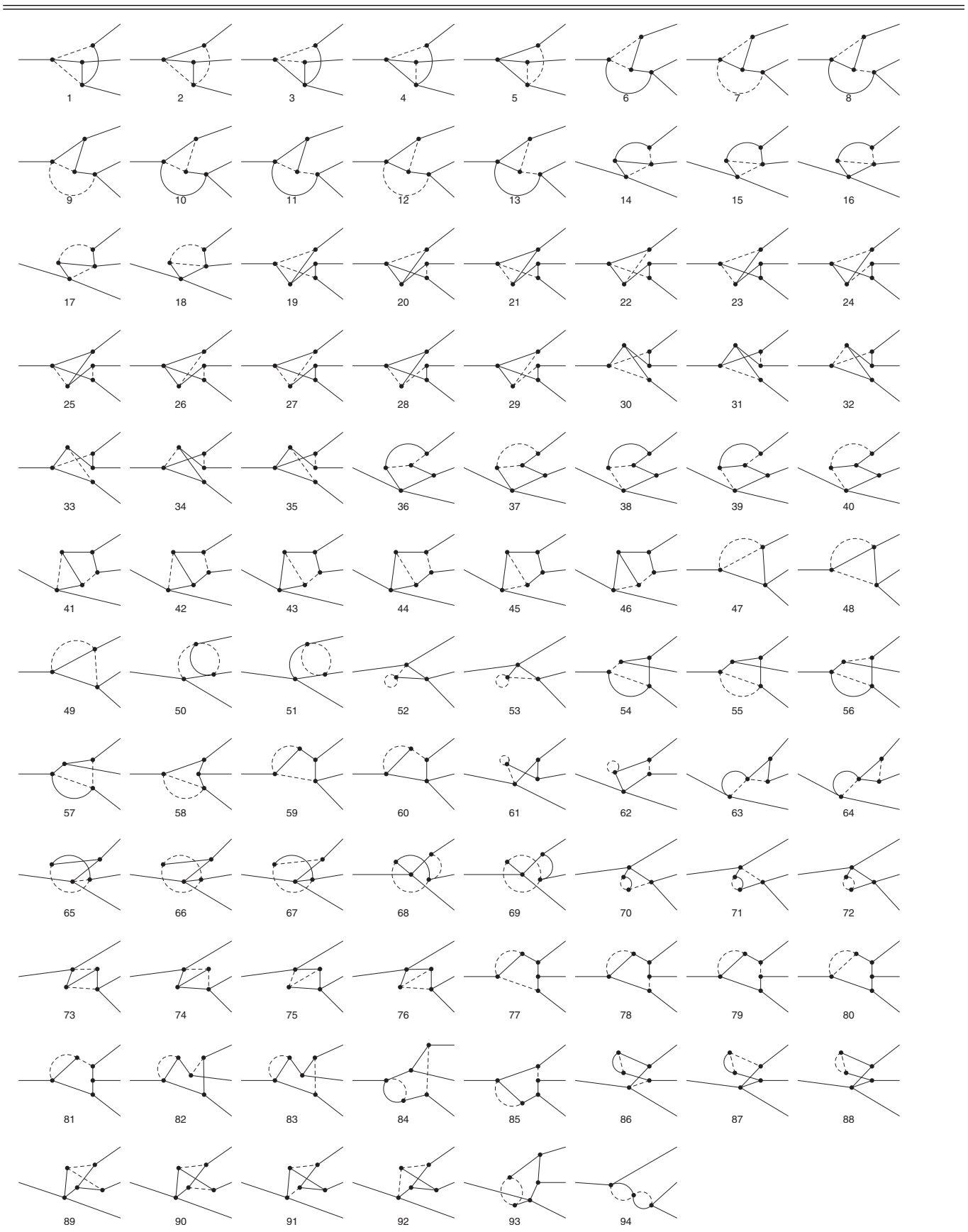


TABLE XIV. Divergent contributions of the diagrams shown in Table XIII.

No.	\mathcal{A}	n	m
1	$\frac{g_1^2 g_2}{g_0}$	-0.0796192	0
2	$\frac{g_1^2 g_2}{g_0}$	0.170381	0
3	$\frac{g_1^2 g_2}{g_0}$	0.0128394	0
4	$\frac{g_1^2 g_2}{g_0}$	-0.0539404	0
5	$\frac{g_1^2 g_2}{g_0}$	0.0582202	0
6	$\frac{g_1(g_0+g_1)g_2}{g_0}$	-0.0398096	0
7	$\frac{g_1(g_0+g_1)g_2}{g_0}$	0.181601	-0.28125
8	$\frac{g_1(g_0+g_1)g_2}{g_0}$	0.0207241	-0.09375
9	$\frac{g_1(g_0+g_1)g_2}{g_0}$	0.185475	-0.28125
10	$\frac{g_1(g_0+g_1)g_2}{g_0}$	0.0851904	0
11	$\frac{g_1(g_0+g_1)g_2}{g_0}$	-0.0289365	-0.09375
12	$\frac{g_1(g_0+g_1)g_2}{g_0}$	-0.486505	0.5625
13	$\frac{g_1(g_0+g_1)g_2}{g_0}$	-0.0769779	0.1875
14	$\frac{g_1(g_0+g_1)g_2}{g_0}$	-0.0539404	0
15	$\frac{g_1(g_0+g_1)g_2}{g_0}$	-0.0796192	0
16	$\frac{g_1(g_0+g_1)g_2}{g_0}$	-0.215762	0
17	$\frac{g_1(g_0+g_1)g_2}{g_0}$	0.0256788	0
18	$\frac{g_1(g_0+g_1)g_2}{g_0}$	0.215762	0
19	$\frac{g_1 g_2^2}{g_0}$	0.0459143	-0.0390625
20	$\frac{g_1 g_2^2}{g_0}$	-0.0800529	0.078125
21	$\frac{g_1 g_2^2}{g_0}$	0.0293269	-0.0390625
22	$\frac{g_1 g_2^2}{g_0}$	-0.108416	0.078125
23	$\frac{g_1 g_2^2}{g_0}$	-0.0206519	0
24	$\frac{g_1 g_2^2}{g_0}$	0.0197361	-0.0234375
25	$\frac{g_1 g_2^2}{g_0}$	-0.00657054	0.078125
26	$\frac{g_1 g_2^2}{g_0}$	0.19079	-0.15625
27	$\frac{g_1 g_2^2}{g_0}$	0.0522647	0
28	$\frac{g_1 g_2^2}{g_0}$	-0.0415526	-0.0234375
29	$\frac{g_1 g_2^2}{g_0}$	-0.0468204	0.046875
30	$\frac{g_1 g_2^2}{g_0}$	0.00918285	-0.0078125
31	$\frac{g_1 g_2^2}{g_0}$	-0.0160106	0.015625
32	$\frac{g_1 g_2^2}{g_0}$	0.00586539	-0.0078125
33	$\frac{g_1 g_2^2}{g_0}$	-0.0216832	0.015625
34	$\frac{g_1 g_2^2}{g_0}$	-0.00131411	0.015625
35	$\frac{g_1 g_2^2}{g_0}$	0.038158	-0.03125
36	$\frac{g_1 g_2^2}{g_0}$	-0.0965356	0
37	$\frac{g_1 g_2^2}{g_0}$	0.0738452	0
38	$\frac{g_1 g_2^2}{g_0}$	0.0175962	-0.0234375
39	$\frac{g_1 g_2^2}{g_0}$	0.0275486	-0.0234375
40	$\frac{g_1 g_2^2}{g_0}$	-0.0650495	0.046875
41	$\frac{(g_0+g_1)g_2^2}{g_0}$	0.0275486	-0.0234375

TABLE XIV. (Continued.)

No.	\mathcal{A}	n	m
42	$\frac{(g_0+g_1)g_2^2}{g_0}$	-0.0480317	0.046875
43	$\frac{(g_0+g_1)g_2^2}{g_0}$	-0.00115712	0.046875
44	$\frac{(g_0+g_1)g_2^2}{g_0}$	0.0125021	-0.046875
45	$\frac{(g_0+g_1)g_2^2}{g_0}$	-0.0206519	0
46	$\frac{(g_0+g_1)g_2^2}{g_0}$	0.0197361	-0.0234375
47	$\frac{g_0^3+2g_1^2g_0+4g_1^3}{g_0}$	-0.107881	0
48	$\frac{g_0^3+2g_1^2g_0+4g_1^3}{g_0}$	0.381554	-0.75
49	$\frac{g_0^3+2g_1^2g_0+4g_1^3}{g_0}$	-0.0249845	-0.375
50	$\frac{g_0^3+2g_1^2g_0+4g_1^3}{g_0}$	0.190777	-0.375
51	$\frac{g_0^3+2g_1^2g_0+4g_1^3}{g_0}$	-0.323643	0
52	$\frac{g_0^3+2g_1g_0^2+2g_1^2g_0+4g_1^3}{g_0}$	0.1875	0
53	$\frac{g_0^3+2g_1g_0^2+2g_1^2g_0+4g_1^3}{g_0}$	0.1875	0
54	$\frac{g_1^2g_2}{g_0}$	0.378277	-0.375
55	$\frac{g_1^2g_2}{g_0}$	-0.136142	0
56	$\frac{g_1^2g_2}{g_0}$	-0.540793	0.75
57	$\frac{g_1^2g_2}{g_0}$	0.0375155	-0.375
58	$\frac{g_1^2g_2}{g_0}$	-0.0453808	0
59	$\frac{g_1^2g_2}{g_0}$	0.787535	-0.84375
60	$\frac{g_1^2g_2}{g_0}$	-0.0125116	0.28125
61	$\frac{g_1(g_0+2g_1)g_2}{g_0}$	0.09375	0
62	$\frac{g_1(g_0+2g_1)g_2}{g_0}$	-0.09375	0
63	$\frac{g_1(2g_0+g_1)g_2}{g_0}$	0.310206	-0.375
64	$\frac{g_1(2g_0+g_1)g_2}{g_0}$	-0.310206	0.375
65	$\frac{g_1^2g_2}{g_0}$	0.756554	-0.75
66	$\frac{g_1^2g_2}{g_0}$	-0.431524	0
67	$\frac{g_1^2g_2}{g_0}$	-0.365785	0.5625
68	$\frac{g_1^2g_2}{g_0}$	-0.540793	0.75
69	$\frac{g_1^2g_2}{g_0}$	0.431524	0
70	$\frac{(g_0^2+2g_1^2)g_2}{g_0}$	0.0914462	-0.140625
71	$\frac{(g_0^2+2g_1^2)g_2}{g_0}$	0.131256	-0.140625
72	$\frac{(g_0^2+2g_1^2)g_2}{g_0}$	0.107881	0
73	$\frac{g_1(2g_0+g_1)g_2}{g_0}$	0.0605337	-0.09375
74	$\frac{g_1(2g_0+g_1)g_2}{g_0}$	0.0207241	-0.09375
75	$\frac{g_1(2g_0+g_1)g_2}{g_0}$	-0.0398096	0
76	$\frac{g_1(2g_0+g_1)g_2}{g_0}$	-0.0414484	0.1875
77	$\frac{g_1g_2^2}{g_0}$	0.267196	-0.210938
78	$\frac{g_1g_2^2}{g_0}$	-0.227387	0.210938
79	$\frac{g_1g_2^2}{g_0}$	0.0549622	-0.0703125
80	$\frac{g_1g_2^2}{g_0}$	-0.0210752	0
81	$\frac{g_1g_2^2}{g_0}$	-0.00920429	0.0703125

TABLE XIV. (Continued.)

No.	\mathcal{A}	n	m
82	$\frac{g_1 g_2^2}{g_0}$	0.24733	-0.316406
83	$\frac{g_1 g_2^2}{g_0}$	-0.151591	0.140625
84	$\frac{g_1 g_2^2}{g_0}$	0.0274811	-0.0351563
85	$\frac{g_1 g_2^2}{g_0}$	-0.0757955	0.0703125
86	$\frac{g_1 g_2^2}{g_0}$	0.0890654	-0.0703125
87	$\frac{g_1 g_2^2}{g_0}$	-0.227387	0.210938
88	$\frac{g_1 g_2^2}{g_0}$	-0.107881	0
89	g_2^2	0.0113452	0
90	g_2^2	-0.0113452	0
91	g_2^2	-0.0141308	0
92	g_2^2	0.0241846	0
93	$\frac{g_1 g_2^2}{g_0}$	0.130571	0
94	$\frac{g_0^3 + 6g_1^2 g_0 + 2g_1^3}{g_0}$	0.432912	-0.75

APPENDIX I: $\Gamma_{1,3}^{1122}(0)$

Table XV shows the one-loop diagrams contributing to $\Gamma_{1,3}^{1122}(0)$ and their respective divergent contributions. The divergent parts of the one-loop diagrams have the general form $r^{-\epsilon/2} u_1 \mathcal{A}(\frac{n}{\epsilon})$.

As the first two diagrams in Table XV cancel each other there is no g_2 contribution to the renormalization constant Z_1 at the one-loop order. Table XVI shows the two-loop diagrams contributing to $\Gamma_{1,3}^{1122}(0)$.

The divergent contributions of the above diagrams to $\Gamma_{1,3}^{1122}(0)$ have the general form $r^{-\epsilon} u_1 \mathcal{A}(\frac{n}{\epsilon} + \frac{m}{\epsilon^2})$. The parameters \mathcal{A} , n and m for each of the above diagrams are listed against their respective diagram numbers in Table XVII.

Collecting the divergences from all the diagrams given in Tables XV and XVI and applying the renormalization condition (13) yields

$$Z_1 = 1 + \frac{1}{\epsilon} \left(\lambda_0 + 2.5\lambda_1 - 0.25\lambda_0^2 - 2.5\lambda_1^2 - 1.5\lambda_0\lambda_1 + 0.0676406\lambda_2\lambda_0 + 0.253861\lambda_1\lambda_2 + 0.00136604\lambda_2^2 - \frac{0.0179802\lambda_2\lambda_0^2}{\lambda_1} - \frac{0.000747121\lambda_2^2\lambda_0}{\lambda_1} \right) + \frac{1}{\epsilon^2} (1.25\lambda_0^2 + 7.75\lambda_1^2 + 3.75\lambda_1\lambda_0 + 0.1875\lambda_2\lambda_0 + 0.46875\lambda_1\lambda_2). \quad (II)$$

All the results obtained in Appendices B to I using the computational method described in Appendix A when truncated to one-loop order agree with the results obtained in Ref. [21], where calculations were performed only to this order.

TABLE XV. One-loop contributions to $\Gamma_{1,3}^{1122}(0)$.

Diagram	\mathcal{A}, n	Diagram	\mathcal{A}, n	Diagram	\mathcal{A}, n
	$\frac{g_0 g_2}{g_1}, 0.125$		$\frac{g_0 g_2}{g_1}, -0.125$		$2g_0 + 5g_1, 0.5$

TABLE XVI. Two-loop diagrams contributing to $\Gamma_{1,3}^{1122}(0)$.

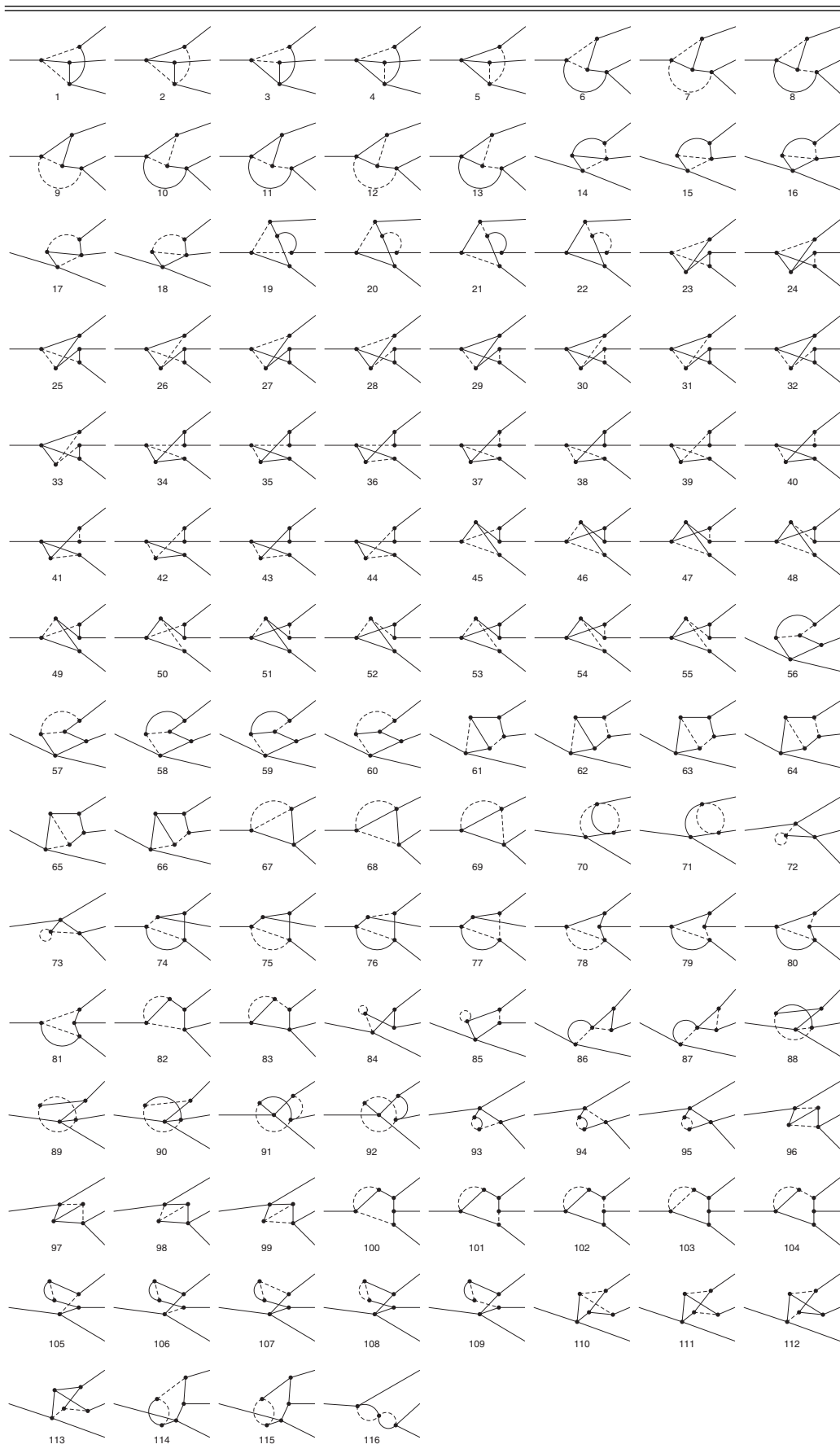


TABLE XVII. Divergent contributions of the diagrams shown in Table XVI.

No.	A	n	m
1	$(g_0 + 4g_1)g_2$	-0.0265397	0
2	$(g_0 + 4g_1)g_2$	0.0567936	0
3	$(g_0 + 4g_1)g_2$	0.00427981	0
4	$(g_0 + 4g_1)g_2$	-0.0179801	0
5	$(g_0 + 4g_1)g_2$	0.0194067	0
6	$(3g_0 + 7g_1)g_2$	-0.00663493	0
7	$(3g_0 + 7g_1)g_2$	0.0302668	-0.046875
8	$(3g_0 + 7g_1)g_2$	0.00345401	-0.015625
9	$(3g_0 + 7g_1)g_2$	0.0309125	-0.046875
10	$(3g_0 + 7g_1)g_2$	0.0141984	0
11	$(3g_0 + 7g_1)g_2$	-0.00482275	-0.015625
12	$(3g_0 + 7g_1)g_2$	-0.0810842	0.09375
13	$(3g_0 + 7g_1)g_2$	-0.0128297	0.03125
14	$(3g_0 + 7g_1)g_2$	-0.00899006	0
15	$(3g_0 + 7g_1)g_2$	-0.0132699	0
16	$(3g_0 + 7g_1)g_2$	-0.0359603	0
17	$(3g_0 + 7g_1)g_2$	0.00427981	0
18	$(3g_0 + 7g_1)g_2$	0.0359603	0
19	g_2^2	-0.00706539	0
20	g_2^2	0.0201538	0
21	g_2^2	0.0161231	0
22	g_2^2	-0.0208333	0
23	$\frac{(g_0+9g_1)g_2^2}{g_1}$	0.00229571	-0.00195313
24	$\frac{(g_0+9g_1)g_2^2}{g_1}$	-0.00400265	0.00390625
25	$\frac{(g_0+9g_1)g_2^2}{g_1}$	0.00146635	-0.00195313
26	$\frac{(g_0+9g_1)g_2^2}{g_1}$	-0.00542079	0.00390625
27	g_2^2	-0.010326	0
28	g_2^2	0.00986803	-0.0117188
29	$\frac{(g_0+9g_1)g_2^2}{g_1}$	-0.000328527	0.00390625
30	$\frac{(g_0+9g_1)g_2^2}{g_1}$	0.00953951	-0.0078125
31	g_2^2	0.0261324	0
32	g_2^2	-0.0207763	-0.0117188
33	g_2^2	-0.0234102	0.0234375
34	$\frac{(3g_0+5g_1)g_2^2}{g_1}$	0.00229571	-0.00195313
35	$\frac{(3g_0+5g_1)g_2^2}{g_1}$	0.00146635	-0.00195313
36	$\frac{(3g_0+5g_1)g_2^2}{g_1}$	-0.00542079	0.00390625
37	$\frac{(3g_0+5g_1)g_2^2}{g_1}$	-0.00400265	0.00390625
38	$\frac{(g_0+g_1)g_2^2}{g_1}$	-0.00344199	0
39	$\frac{(g_0+g_1)g_2^2}{g_1}$	0.00328934	-0.00390625
40	$\frac{(3g_0+5g_1)g_2^2}{g_1}$	-0.000328527	0.00390625
41	$\frac{(3g_0+5g_1)g_2^2}{g_1}$	0.00953951	-0.0078125
42	$\frac{(g_0+g_1)g_2^2}{g_1}$	-0.00692543	-0.00390625
43	$\frac{(g_0+g_1)g_2^2}{g_1}$	0.00871079	0
44	$\frac{(g_0+g_1)g_2^2}{g_1}$	-0.00780339	0.0078125
45	g_2^2	0.00459143	-0.00390625
46	g_2^2	-0.00344199	0
47	g_2^2	-0.00800529	0.0078125
48	g_2^2	0.00328934	-0.00390625

TABLE XVII. (Continued.)

No.	\mathcal{A}	n	m
49	g_2^2	0.00293269	-0.00390625
50	g_2^2	-0.0108416	0.0078125
51	g_2^2	-0.000657054	0.0078125
52	g_2^2	-0.00692543	-0.00390625
53	g_2^2	0.00871079	0
54	g_2^2	0.019079	-0.015625
55	g_2^2	-0.00780339	0.0078125
56	$\frac{(g_0+3g_1)g_2^2}{g_1}$	-0.0160893	0
57	$\frac{(g_0+3g_1)g_2^2}{g_1}$	0.0123075	0
58	$\frac{(g_0+3g_1)g_2^2}{g_1}$	0.00293269	-0.00390625
59	$\frac{(g_0+3g_1)g_2^2}{g_1}$	0.00459143	-0.00390625
60	$\frac{(g_0+3g_1)g_2^2}{g_1}$	-0.0108416	0.0078125
61	$\frac{(g_0+5g_1)g_2^2}{g_1}$	0.00459143	-0.00390625
62	$\frac{(g_0+5g_1)g_2^2}{g_1}$	-0.00800529	0.0078125
63	$\frac{(g_0+5g_1)g_2^2}{g_1}$	-0.000192854	0.0078125
64	$\frac{(g_0+5g_1)g_2^2}{g_1}$	0.00208369	-0.0078125
65	$\frac{(g_0+5g_1)g_2^2}{g_1}$	-0.00344199	0
66	$\frac{(g_0+5g_1)g_2^2}{g_1}$	0.00328934	-0.00390625
67	$g_0^2 + 6g_1g_0 + 10g_1^2$	-0.0359603	0
68	$g_0^2 + 6g_1g_0 + 10g_1^2$	0.127185	-0.25
69	$g_0^2 + 6g_1g_0 + 10g_1^2$	-0.00832817	-0.125
70	$g_0^2 + 6g_1g_0 + 10g_1^2$	0.0635923	-0.125
71	$g_0^2 + 6g_1g_0 + 10g_1^2$	-0.107881	0
72	$2g_0^2 + 9g_1g_0 + 10g_1^2$	0.0625	0
73	$2g_0^2 + 9g_1g_0 + 10g_1^2$	0.0625	0
74	$\frac{(g_0^2+4g_1g_0+6g_1^2)g_2}{g_1}$	0.0157615	-0.015625
75	$\frac{(g_0^2+8g_1g_0+18g_1^2)g_2}{g_1}$	-0.00378173	0
76	$\frac{(g_0^2+4g_1g_0+6g_1^2)g_2}{g_1}$	-0.022533	0.03125
77	$\frac{(g_0^2+4g_1g_0+6g_1^2)g_2}{g_1}$	0.00156315	-0.015625
78	$\frac{(g_0^2+8g_1^2)g_2}{g_1}$	-0.00378173	0
79	$\frac{(g_0^2+8g_1^2)g_2}{g_1}$	0.00156315	-0.015625
80	$\frac{(g_0^2+8g_1^2)g_2}{g_1}$	-0.022533	0.03125
81	$\frac{(g_0^2+8g_1^2)g_2}{g_1}$	0.0157615	-0.015625
82	$(g_0 + 3g_1)g_2$	0.131256	-0.140625
83	$(g_0 + 3g_1)g_2$	-0.00208527	0.046875
84	$\frac{(g_0^2+5g_1g_0+6g_1^2)g_2}{g_1}$	0.015625	0
85	$\frac{(g_0^2+5g_1g_0+6g_1^2)g_2}{g_1}$	-0.015625	0
86	$\frac{(g_0^2+2g_1g_0+7g_1^2)g_2}{g_1}$	0.051701	-0.0625
87	$\frac{(g_0^2+2g_1g_0+7g_1^2)g_2}{g_1}$	-0.051701	0.0625
88	$(g_0 + 3g_1)g_2$	0.126092	-0.125
89	$(g_0 + 3g_1)g_2$	-0.0719206	0
90	$(g_0 + 3g_1)g_2$	-0.0609641	0.09375
91	$(g_0 + 3g_1)g_2$	-0.0901321	0.125
92	$(g_0 + 3g_1)g_2$	0.0719206	0

TABLE XVII. (Continued.)

No.	\mathcal{A}	n	m
93	$(2g_0 + 5g_1)g_2$	0.0304821	-0.046875
94	$(2g_0 + 5g_1)g_2$	0.0437519	-0.046875
95	$(2g_0 + 5g_1)g_2$	0.0359602	0
96	$\frac{(g_0^2+2g_1g_0+7g_1^2)g_2}{g_1}$	0.0100889	-0.015625
97	$\frac{(g_0^2+2g_1g_0+7g_1^2)g_2}{g_1}$	0.00345401	-0.015625
98	$\frac{(g_0^2+2g_1g_0+7g_1^2)g_2}{g_1}$	-0.00663493	0
99	$\frac{(g_0^2+2g_1g_0+7g_1^2)g_2}{g_1}$	-0.00690807	0.03125
100	$\frac{(g_0+5g_1)g_2^2}{g_1}$	0.0148442	-0.0117188
101	g_2^2	-0.0757955	0.0703125
102	g_2^2	0.0549622	-0.0703125
103	g_2^2	-0.00702507	0
104	g_2^2	-0.0030681	0.0234375
105	$\frac{(g_0+3g_1)g_2^2}{g_1}$	0.0148442	-0.0117188
106	$\frac{(g_0+3g_1)g_2^2}{g_1}$	0.0148442	-0.0117188
107	$\frac{(g_0+3g_1)g_2^2}{g_1}$	-0.0378978	0.0351563
108	$\frac{(g_0+3g_1)g_2^2}{g_1}$	-0.0179801	0
109	$\frac{(g_0+3g_1)g_2^2}{g_1}$	-0.0378978	0.0351563
110	g_2^2	0.0113452	0
111	g_2^2	-0.0113452	0
112	g_2^2	-0.0141308	0
113	g_2^2	0.0120923	0
114	$\frac{(g_0+3g_1)g_2^2}{g_1}$	0.0274811	-0.0351563
115	$\frac{(g_0+3g_1)g_2^2}{g_1}$	0.0217619	0
116	$3g_0^2 + 3g_1g_0 + 11g_1^2$	0.144304	-0.25

[1] G. Ódor, *Rev. Mod. Phys.* **76**, 663 (2004).
 [2] U. C. Täuber, *Critical Dynamics: A Field Theory Approach to Equilibrium and Non-Equilibrium Scaling Behavior* (Cambridge University, Cambridge, England, 2014).
 [3] N. Antonov, N. Gulitskiy, P. Kakin, and V. Serov, [arXiv:2005.04756](https://arxiv.org/abs/2005.04756) (2020).
 [4] J. T. Young, A. V. Gorshkov, M. Foss-Feig, and M. F. Maghrebi, *Phys. Rev. X* **10**, 011039 (2020).
 [5] B. Schmittmann and R. Zia, in *Phase Transitions and Critical Phenomena*, edited by C. Domb and J. Lebowitz (Academic, London, 1995), Vol. 17.
 [6] U. C. Täuber, J. E. Santos, and Z. Rácz, *Eur. Phys. J. B* **7**, 309 (1999).
 [7] W. Kinzel, in *Percolation Structures and Processes*, edited by R. Z. G. Deutscher and J. Adler (Hilger, Bristol, 1983), Vol. 5.
 [8] H.-K. Janssen, *Z. Phys. B* **42**, 151 (1981).
 [9] S.-K. Ma, *Modern Theory of Critical Phenomena* (Routledge, New York, 2018).
 [10] P. C. Hohenberg and B. I. Halperin, *Rev. Mod. Phys.* **49**, 435 (1977).
 [11] S. Katz, J. L. Lebowitz, and H. Spohn, *Phys. Rev. B* **28**, 1655 (1983).
 [12] S. Katz, J. L. Lebowitz, and H. Spohn, *J. Stat. Phys.* **34**, 497 (1984).
 [13] D. Helbing, *Rev. Mod. Phys.* **73**, 1067 (2001).
 [14] D. Chowdhury, L. Santen, and A. Schadschneider, *Phys. Rep.* **329**, 199 (2000).
 [15] L. M. Sieberer, S. D. Huber, E. Altman, and S. Diehl, *Phys. Rev. B* **89**, 134310 (2014).
 [16] U. C. Täuber and S. Diehl, *Phys. Rev. X* **4**, 021010 (2014).
 [17] H. D. Vuijk, R. Rens, M. Vahabi, F. C. MacKintosh, and A. Sharma, *Phys. Rev. E* **91**, 032143 (2015).
 [18] H. Janssen and B. Schmittmann, *Z. Phys. B* **64**, 503 (1986).
 [19] B. Schmittmann and K. E. Bassler, *Phys. Rev. Lett.* **77**, 3581 (1996).
 [20] K. E. Bassler and B. Schmittmann, *Phys. Rev. E* **49**, 3614 (1994).
 [21] S. B. Dutta and S.-C. Park, *Phys. Rev. E* **83**, 011117 (2011).
 [22] K.-t. Leung and J. L. Cardy, *J. Stat. Phys.* **44**, 567 (1986).
 [23] V. Becker and H. Janssen, *Europhys. Lett.* **19**, 13 (1992).
 [24] P. C. Martin, E. D. Siggia, and H. A. Rose, *Phys. Rev. A* **8**, 423 (1973).
 [25] U. C. Täuber and F. Schwabl, *Phys. Rev. B* **46**, 3337 (1992).
 [26] R. Zia and B. Schmittmann, *J. Stat. Mech.* (2007) P07012.

- [27] T. Chou, K. Mallick, and R. Zia, *Rep. Prog. Phys.* **74**, 116601 (2011).
- [28] K. E. Bassler and B. Schmittmann, *Phys. Rev. Lett.* **73**, 3343 (1994).
- [29] T. Hahn, *Comput. Phys. Commun.* **140**, 418 (2001).
- [30] R. Mertig, M. Böhm, and A. Denner, *Comput. Phys. Commun.* **64**, 345 (1991).
- [31] V. Shtabovenko, R. Mertig, and F. Orellana, *Comput. Phys. Commun.* **207**, 432 (2016).
- [32] Wolfram Research, Inc., *Mathematica*, Version 11.1 (Wolfram Research, Inc., Champaign, Illinois, 2017).
- [33] J. Carter and G. Heinrich, *Comput. Phys. Commun.* **182**, 1566 (2011).
- [34] W. Bruns, B. Ichim, T. Römer, R. Sieg, and C. Söger, Normaliz. Algorithms for rational cones and affine monoids, (2010), <http://www.math.uos.de/normaliz>.
- [35] W. Bruns, B. Ichim, and C. Söger, [arXiv:1206.1916](https://arxiv.org/abs/1206.1916) (2012).
- [36] V. Becker and H. Janssen, *J. Stat. Phys.* **96**, 817 (1999).